Quenching of the relaxation pathway in the Weyl semimetal TaAs

Jiayun Liu,[1] Liang Cheng,[1,2] Daming Zhao,[1] Xiaoxuan Chen,[1] Handong Sun,[1] Zhilin Li,[3] Xinbo Wang,[3] Jian-Xin Zhu,[4,*] and Elbert E. M. Chia[1,†]

[1]*Division of Physics and Applied Physics, School of Physical and Mathematical Sciences, Nanyang Technological University, 21 Nanyang Link, Singapore 637371*

[2]*State Key Laboratory of Electronic Thin Films and Integrated Devices University of Electronic Science and Technology of China, Chengdu 610054, China*

[3]*Beijing National Laboratory for Condensed Matter Physics, Institute of Physics, Chinese Academy of Sciences, Beijing 100190, China*

[4]*Theoretical Division and Center for Integrated Nanotechnologies, Los Alamos National Laboratory, Los Alamos, New Mexico 87545, USA*

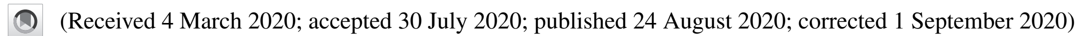

(Received 4 March 2020; accepted 30 July 2020; published 24 August 2020; corrected 1 September 2020)

Since tantalum arsenide (TaAs) has been experimentally verified as a Weyl semimetal, intensive research has been devoted to study of the unique properties of the material. Despite this, the ultrafast dynamics of TaAs is still not very well understood. In this work, we study the relaxation dynamics in TaAs using transient reflection spectroscopy. From the transient reflection measurement, we observe either a single (fast) or a dual (fast and slow) relaxation, depending on the probing wavelength. The additional relaxation channel is attributed to an asymmetric population of photoexcited electrons and holes.

DOI: 10.1103/PhysRevB.102.064307

I. INTRODUCTION

Topological insulators are unique materials with insulating bulk states as well as spin-polarized conducting surface states that are topologically protected [1–3]. Due to this unique electronic property, topological insulators have seen a plethora of applications such as in broadband photodetectors [4–6] and spin current injection [7,8] and detection [9,10]. Following the topological classification of materials, Dirac semimetal has been predicted theoretically [11] and has since been experimentally confirmed through mapping of the band structure by angle-resolved photoemission spectroscopy (ARPES) [12,13]. This Dirac semimetal has gapless dispersion at certain points in momentum space known as Dirac points. These three-dimensional (3D) Dirac points have been experimentally observed in Cd_3As_2 [12] and BiO_2 [14] crystals. There are doubly degenerate states on these Dirac points [15], which can be lifted if either the time reversal symmetry $\mathcal{T}$ or the inversion symmetry $\mathcal{I}$ is broken [16]. Breaking of either $\mathcal{T}$ or $\mathcal{I}$ results in splitting of the Dirac point into a pair of Weyl nodes in momentum space [17]. This splitting leads to the formation of a Weyl semimetal which corresponds to a new topological phase with fascinating properties like topologically protected Fermi arc states [18,19] and chiral anomaly [20].

The Weyl nodes separated in momentum space each have a well-defined chirality of either $\chi = +1$ or $\chi = -1$ [21]. This well-defined chirality gives rise to a chirality selection rule where right-circularly polarized light is able to excite electrons from the positive k side of the $\chi = +1$ Weyl cone but not the negative side, and vice versa. The energy to excite electrons from the valence band to the conduction band is different for electrons on the positive and the negative k sides of the Weyl cone. Therefore, circular dichroism can be achieved in a Weyl semimetal through the selective excitation of electrons in the Weyl cones. Through the manipulation of circular dichroism, the optical response in the midinfrared regime has been experimentally demonstrated [22] in tantalum arsenide (TaAs), a type I Weyl semimetal [23]. Exploiting the gapless dispersion in TaAs, further experiments have reported a broad bandwidth response of TaAs from the visible to the midinfrared regime [24]. This wide spectral bandwidth of TaAs is ideally suited for application in optoelectronics.

The unique topological properties of TaAs may be the reason for the large second-order nonlinear susceptibility coefficient [25], which gives rise to physical observations like a large second harmonic generation [26] and large photocurrent [27]. Besides the aforementioned properties, TaAs has a large absorption coefficient [28] and high carrier mobility [29]. These properties are present independent of the thickness of TaAs since it is a 3D material unlike transitional metal dichalcogenides [30] and graphene [31] where the material properties are layer dependent. The combination of these properties has made TaAs a potential material for applications in high-sensitivity photodetectors [24] and field-effect transistors [32]. Despite the vast research interest, the transient dynamics of TaAs is not well understood, with the literature reporting different decay dynamics (single-decay dynamics [33] and multiple-decay dynamics [34]) for TaAs. However, knowledge of the transient dynamics is crucial since it determines the response time of the material, which is especially important in ultrafast optoelectronics.

In this work, we studied the ultrafast response of TaAs in the optical regime through transient reflection spectroscopy

*Corresponding author: jxzhu@lanl.gov

†Corresponding author: elbertchia@ntu.edu.sg

 ©2020 American Physical Society

with varying pump fluences. We noted a slow and a fast relaxation for the hot injected electrons in TaAs by the pump pulse. We attributed the fast decay to electron-hole (e-h) recombination, which occurs on the picosecond (ps) time scale. We attributed the slower decay, occurring in tens of ps, to carrier cooling via electron-phonon (e-ph) coupling.

II. METHOD

TaAs crystals were grown by the chemical vapor transport method using iodine as the transport agent. In a typical run, tantalum, arsenic, and a small amount of iodine were loaded into a silica ampoule. The ampoule was evacuated, sealed, and heated slowly to 1050 °C and then subjected to a temperature gradient from 1030 °C to 1070 °C, where the chemical vapor transport proceeded for 2 weeks. TaAs then reacts with iodine at the cooler end, forming gaseous species, is transported to the hotter end, and finally recrystallizes into millimeter-sized TaAs single crystals. More details on the crystal growth can be found in [35].

Transient reflection (TR) spectroscopy is a pump-probe technique to probe excited-state dynamics. Our TR measurement is performed using HELIOS Fire (Ultrafast Systems LLC). A Ti:sapphire laser (Coherent Legend Elite) with a central wavelength at 800 nm, pulse duration of 30 fs, and repetition rate of 1 kHz was used as both the pump and the generator of the white-light probe. The white-light probe allows for the probing of electron filling at different k points of the conduction band. The laser is split into two paths for TR spectroscopy. The white-light probe pulse is generated by focusing the laser from one path onto a sapphire crystal. The copolarized pump and probe pulse are focused on the TaAs sample with spot sizes of 115 and 100 μm, respectively. The spectrum of the reflected probe pulse is measured at different pump-probe delays. The normalized change in reflectance ($\Delta R/R$) at different pump-probe delays is recorded and the TR spectra plotted. The absorption spectrum of TaAs is measured at room temperature with variable-angle spectroscopic ellipsometry (J. A. Woollam Co.).

III. RESULTS

The steady-state absorption spectrum of the Weyl semimetal TaAs measured at room temperature is shown in Fig. 1. The two absorption peaks, at 440 nm (2.82 eV) and 560 nm (2.21 eV), are consistent with calculated band structures reported in the literature [28]; the 440-nm peak corresponds to the transition from –0.2 to 2.6 eV at the N point, while the 560-nm peak corresponds to the transition from –1 to 1.1 eV at the Z point.

To probe the ultrafast dynamics of the Weyl semimetal in the visible regime, the TaAs is excited with an 800-nm pump and probed from 430 to 720 nm at room temperature. The pseudocolor TR spectrum plot of $\Delta R/R$ is displayed in Fig. 2. The spectrum exhibits a positive $\Delta R/R$ signal for probe wavelengths between 500 and 600 nm. The positive $\Delta R/R$ signal corresponds to the process of photobleaching (PB), where the states in the conduction band that were filled with valence-band electrons absorbing the pump pulse can no longer be filled by a subsequent probe pulse. This results in a smaller absorption, and thus a larger reflection, than without the pump. For probe wavelengths outside this range, the TR signal is initially negative, then changes to positive on a ps time scale. The negative signal corresponds to photoinduced absorption, where the electrons are further excited by the probe pulse to higher-energy states after the pump excitation.

From the TR spectra, the excited-state dynamics can be probed by examining the kinetic trace of the probe wavelength. In Fig. 2, the strong PB signal at the 560-nm probe has a transient signal that lasts tens of ps. Compared to the 525-nm probe, which decays within a few ps, the slow decay corresponds to an additional relaxation channel that is absent at the 525-nm probe, which is further discussed below. Therefore,

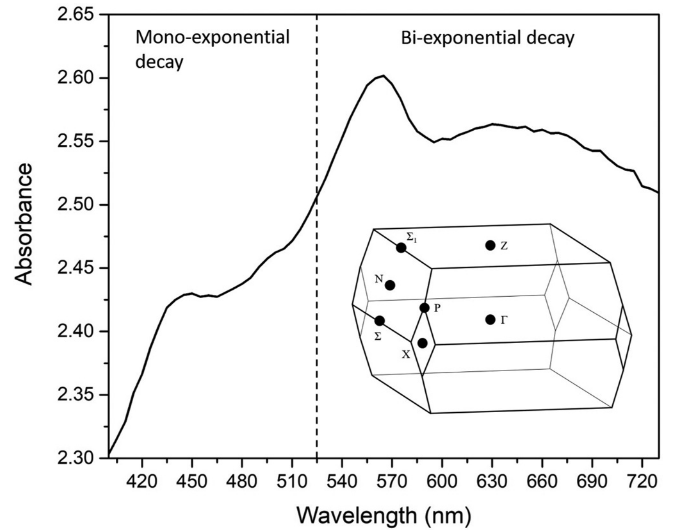

FIG. 1. Steady-state absorption spectrum of TaAs measured by variable-angle spectroscopic ellipsometry at room temperature. Dashed vertical lines separate regions where the TR probe can be fitted with a mono-/biexponential decay function. Absorption peaks at 440 and 560 nm correspond to the transition at the N and Z points, respectively. Inset: First Brillouin zone of TaAs.

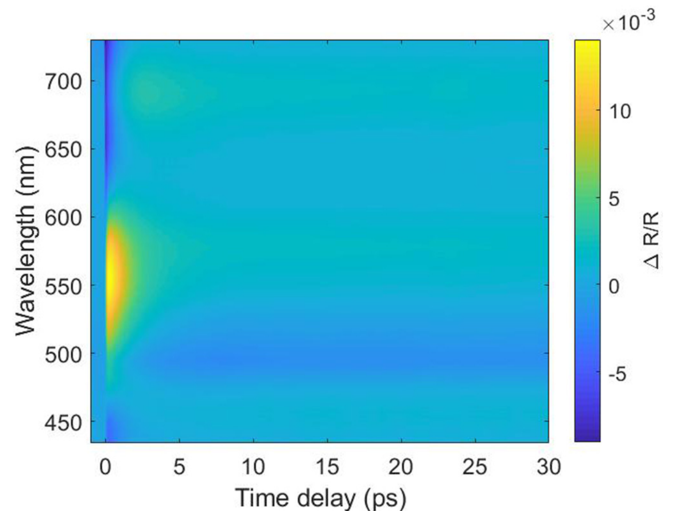

FIG. 2. Pseudocolor TR spectrum plot for TaAs excited with an 800-nm pump at a pump fluence of 480 μJ/cm^2.

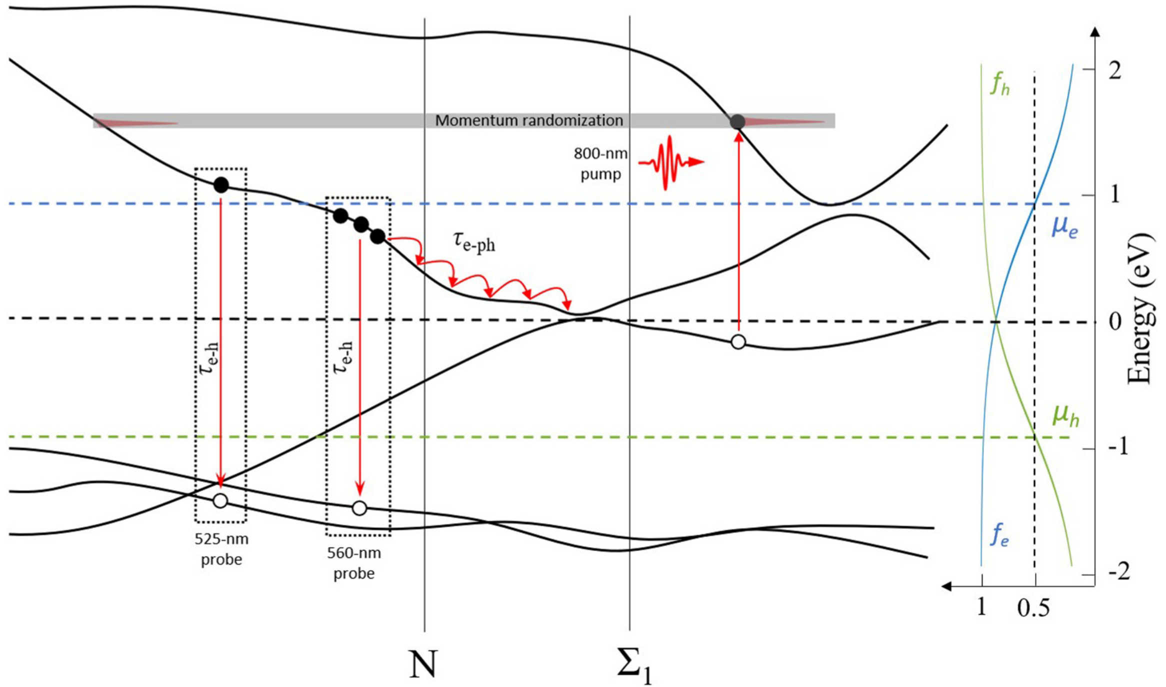

FIG. 3. Realistic band structure schematic of TaAs calculated with density functional theory using the Perdew-Burke-Ernzerhof exchange-correlation functional (including spin-orbit coupling) [28], depicting the asymmetric populations of electrons (filled circles) and holes (open circles) after thermalization. Dotted boxes indicate regions corresponding to 525- and 560-nm absorption.

probing at 560 nm should provide additional dynamics not present at the 525-nm probe. The PB signal can be understood as the occupation of the excited state due to pump excitation as depicted by the filled circles in Fig. 3. The absorption of the probe light is reduced as the higher-energy states are occupied, which increases the transient reflectivity, giving the PB signal. To obtain the relaxation time of the excited state, the kinetic trace is fitted with exponential decay. From the TR spectra, we found out that the 560-nm probe can be fitted with biexponential decay while the 525-nm probe can be fitted with monoexponential decay. The result of the biexponential decay fitting is a fast ($\tau_{\text{fast}} = 1.55 \pm 0.01$ ps) and a slow ($\tau_{\text{slow}} = 190 \pm 10$ ps) decay component as depicted in Fig. 4(a). The monoexponential decay gives a fast ($\tau_{\text{fast}} = 1.59 \pm 0.01$ ps) decay component, as depicted in Fig. 4(b), which is comparable to the fast relaxation obtained previously using the 560-nm probe. This suggests that the single relaxation channel at the 525-nm probe shares the same mechanism as the fast relaxation observed for the 560-nm probe.

To understand the origin of the fast decay, we compare the transient dynamics with that of the traditional semimetal bismuth (Bi). For Bi, the conduction and valence band extrema are at different k points, so e-h recombination is mediated by phonons [36]. The e-h recombination dynamics in Bi has been reported to be in the few-ps range from 2D optical-pump terahertz-probe [37] and optical-pump optical-probe [36] measurements. This establishes the upper limit of the e-h recombination time in TaAs since, in TaAs, e-h recombination does not require mediation by phonons, as the conduction and valence bands overlap at the same k point. Also, the time scale of the fast decay is consistent with e-h recombination in TaAs reported in the literature by transient grating measurement [34], which is sensitive to the density of photoexcited carriers. Furthermore, this time scale is also similar to the reported recombination time ($\sim$1 ps) in graphene [38,39], which has gapless dispersion similar to that of TaAs. Therefore, we ascribe the fast decay component, $\tau_{\text{fast}} = 1.55 \pm 0.01$ ps, to e-h recombination as depicted by $\tau_{\text{e-h}}$ in Fig. 3.

The slow component, which decays in a few tens of ps, could be due to either e-ph coupling or Auger recombination (AR), which occurs on a similar time scale [40,41]. In e-ph coupling, electrons in higher excited states relax through the emission of phonons. AR is a nonradiative process involving three carriers where energy released by an electron-hole recombination is absorbed by either an electron or a hole which is subsequently excited to a higher-energy state. To understand the origin of this slower relaxation, we performed TR spectroscopy at different pump fluences. The kinetics at 560 nm under different pump fluences is shown in Fig. 5(a). Fitting the kinetic traces under different pump fluences, the fast and slow relaxation times obtained are shown in Fig. 5(b). In Fig. 5(b) it is clear that both the fast and the slow relaxation times increase with increasing pump fluence corresponding to a higher initial carrier density. In AR, the relaxation time should *decrease* with increasing carrier population, since more carriers are able to participate in the relaxation process. However, our data show an opposite trend, suggesting that it is not due to AR. In e-ph coupling, on the other hand, the low density of states (DOS) near $E = 0$ [34] limits the carriers relaxing past these states. As the photocarrier population increases with increasing pump fluence, the relaxation time increases, as more carriers are required to scatter past these

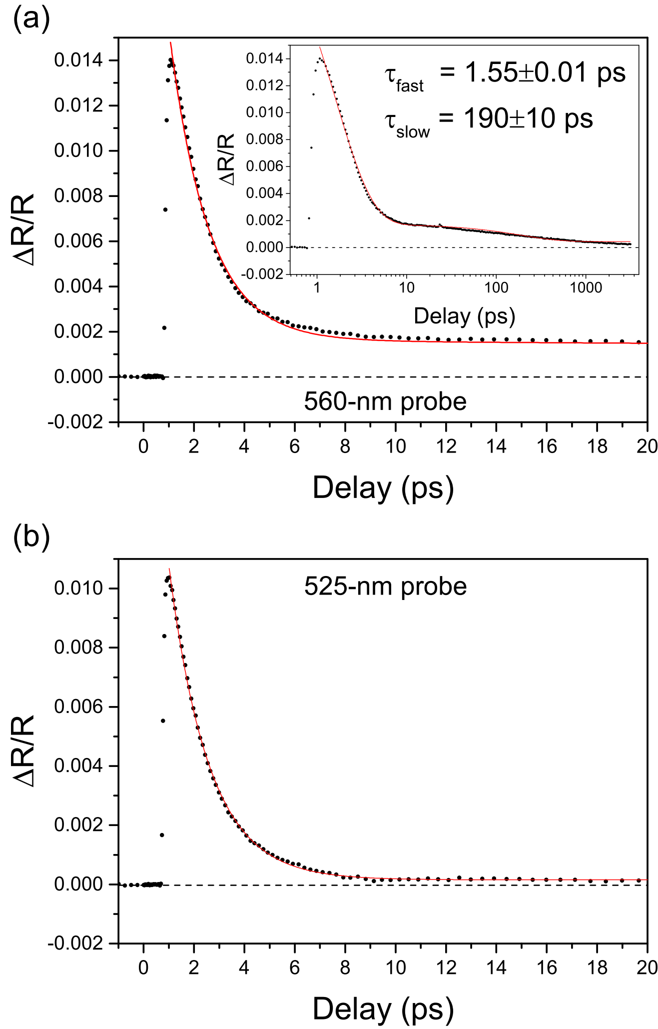

FIG. 4. Experimental data (filled circles) fitted with exponential decay (solid line) for (a) a 560-nm probe and (b) a 525-nm probe under 480 μJ/cm^2 pump fluence. The dashed line represents the data before the pump.

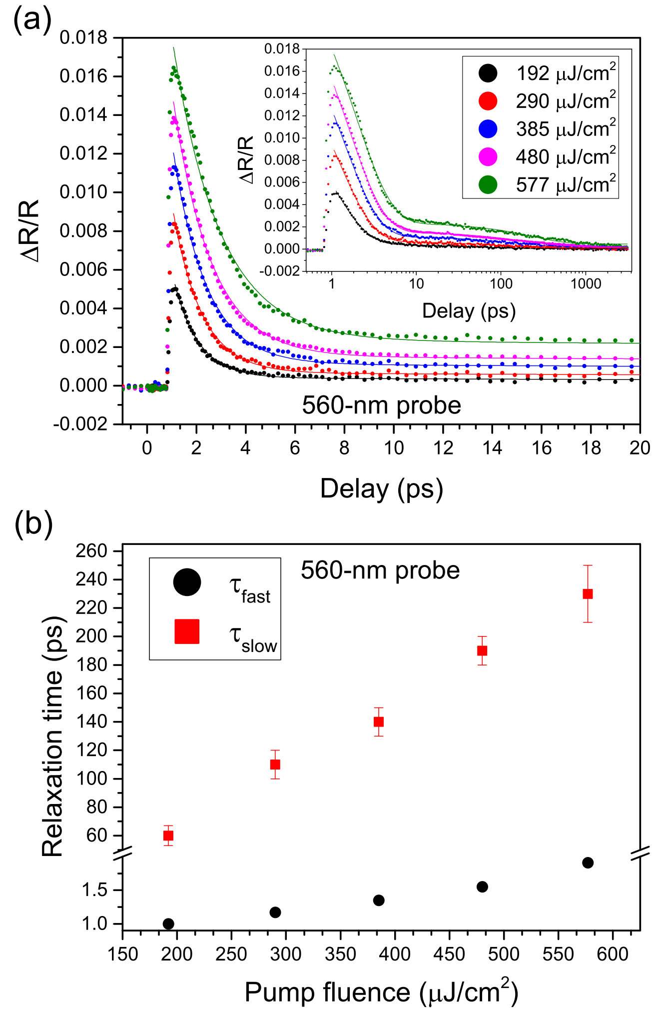

FIG. 5. (a) Experimental data (filled circles) fitted with biexponential decay (solid line). Multiple kinetics at a 560-nm probe wavelength under different pump fluences. Inset: Kinetics at a longer pump probe delay. (b) Relaxation time under different pump fluences.

states with low DOS. Therefore, the relaxation time should *increase* with increasing carrier population [40]. Therefore, the fluence-dependent data suggest that the slower relaxation is due to e-ph coupling. The time scale of e-ph coupling observed is much slower compared to that in a semiconductor, which is typically a few ps [42]. We note that in a semiconductor with a wide bandgap, the recombination time is very long. This slower relaxation in TaAs could be explained [28] by the reduced DOS near $E = 0$; during relaxation, the carriers have to scatter past these states with low DOS before relaxing to the lower-energy states. However, the low DOS restrict the number of carriers that can scatter to the low-energy states, thus forming a bottleneck to the relaxation process. This phenomenon is not observed in a semiconductor since relaxation is through intraband transition where such a bottleneck is not present.

We obtained two relaxation time scales (τ_{fast} and τ_{slow}) from the fitting result of the 560-nm probe but a single relaxation time scale (τ_{fast}) from the 525-nm probe. We attribute the fast decay component to e-h recombination and the slow decay to e-ph coupling. The absence of the slow decay component at the 525-nm probe is further discussed in the following section.

IV. DISCUSSION

A. Dual relaxation channels in TaAs

The fluence-dependent data suggest that the hot-electron dynamics is similar to that of semiconductors. The optical pump pulse excites the electrons far above the Weyl nodes into a nonthermal distribution. These electrons subsequently undergo momentum randomization [43] and thermalization via electron-electron scattering on the tens-of-femtoseconds time scale [34], resulting in the electron and hole distribution following a Fermi-Dirac distribution $f_e(E)$ and $f_h(E)$, respectively, over all allowed k vectors in the entire Brillouin zone. These electrons in excited states then relax to the ground state through e-h recombination. This transition corresponds

to $\tau_{\text{e-h}}$, which we observed in our experiment as illustrated in Fig. 3. Although this physical picture has been able to explain the carrier dynamics in various materials like semiconductors [38] and perovskites [40], it does not provide an explanation for dual relaxation in TaAs. It does not explain the electrons' relaxing via a second, slower relaxation channel instead of just following the faster and more efficient relaxation channel. This problem can be explained by looking at the carrier population immediately after thermalization, which can be deduced indirectly from the steady-state absorption spectra. The absorption spectra tell us the joint density of states (JDOS) for different probe wavelengths: A higher JDOS corresponds to a wider range of k vectors where optical transitions are possible, as depicted by the wider dotted box in the left portion of Fig. 3. Hence a higher JDOS corresponds to more available excited states for the electrons to scatter to during thermalization. In addition, the chemical potentials of electrons (μ_{e}) and holes (μ_{h}) after thermalization are at different energies, which are estimated from $N_{\text{e/h}} = \int_0^\infty dE\, f_{\text{e/h}}(E) g_{\text{e/h}}(E)$, where $g_{\text{e/h}}(E)$ is the DOS in the conduction/valence band for the electron/hole, in the parabolic-band approximation. From the Fermi-Dirac function, we see that states below μ_e are filled with electrons while states above μ_h are filled with holes. Hence, the occupation factor of *holes* below μ_h is small, implying a low concentration of holes in these states. This results in an asymmetric population of electrons and holes as depicted in Fig. 3. Recombination of the excited electrons to the lower-energy hole states is thus limited by the low hole concentration at these states. Therefore, the remaining excited-state electrons can only relax via other channels.

Besides comparing the fast decay time scale to the reported recombination time in semimetals, we further verify that the fast decay corresponds to recombination by comparing the fluence-dependent results with the literature. Since the band structure of graphene is similar to those of Weyl semimetals, the fluence dependence of the relaxation times should be similar to that of TaAs. The recombination time in graphene has been reported to exhibit a positive correlation with the carrier density [39], consistent with our fluence-dependent τ_{fast} in TaAs as shown in Fig. 5. As the pump fluence increases, more carriers are generated, increasing the carrier density where the recombination time is expected to increase.

At the same time, hot electrons can relax through an additional relaxation channel, namely, carrier cooling via e-ph coupling as denoted by $\tau_{\text{e-ph}}$ in Fig. 3. This relaxation mechanism is slower than the recombination lifetime for the following reasons. First, the photoexcited electrons are required to scatter past the $E = 0$ states (near Σ_1 in Fig. 3) before relaxing to the lower-energy states [34]. However, the low DOS limits this relaxation process and thus increases the relaxation time. Second, the relaxation to different k points via e-ph coupling requires the emission of phonons. However, these electrons can subsequently reabsorb the phonons, thus slowing down the electron cooling process [40]. This explanation is consistent with our pump fluence data in Fig. 5(b). As the pump fluence increases, the density of the photoexcited hot carriers increases, which, during relaxation, causes the emission of a larger number of phonons; this in turn increases the reabsorption of phonons by the carriers, which ultimately increases the relaxation time τ_{slow}. Since e-h recombination does not require scattering past states with a low DOS or phonon emission, e-h recombination can be more efficient than e-ph coupling in TaAs. Therefore, the combination of a low DOS and phonon reabsorption by the carriers makes e-ph coupling an inefficient relaxation mechanism compared to e-h recombination.

B. Quenching of electron-phonon coupling

From the steady-state absorption spectrum in Fig. 1, we see that starting at 475 nm, absorption increases with increasing wavelength and peaks at 560 nm. Above a certain absorption threshold (~2.51 in Fig. 1) corresponding to a probe wavelength longer than ~525nm, there is a larger JDOS between the initial and the final states. The majority of the photoexcited electrons thus thermalize and occupy regions in k space corresponding to these "final" states (from steady-state absorption data) with high JDOS, then start their cooling process by the dual channels of e-h recombination and e-ph coupling. On the other hand, the JDOS is lower for probe wavelengths shorter than ~525 nm. This corresponds to regions of k space where there are fewer thermalized hot electrons, and so the electrons should be able to relax entirely through the more efficient e-h recombination as depicted schematically by the narrower dotted box at the left in Fig. 3. This picture is consistent with our experimental observation of a single-exponential relaxation for probe wavelengths shorter than 525 nm and double-exponential relaxation for probe wavelengths longer than 525 nm. Interestingly, we can see that for probe wavelengths longer than 525 nm, there is a very long-lived (~ns) constant offset, which may be related to carriers that have already relaxed to the Dirac point: There the vanishingly low DOS makes further relaxation extremely inefficient. The kinetics at the 525-nm probe can be fitted well with a monoexponential decay, shown in Fig. 4(b), with a relaxation time of (1.59 ± 0.01) ps. Also, the absence of the slow decay due to e-h coupling at the 525-nm probe is consistent with our physical model described above.

From classical electrodynamics, the current density is proportional to the carrier density of the photogenerated electrons/holes in the conduction/valence band. However, how long this photoinduced current can be sustained depends on how fast these photocarriers relax or recombine [44,45]. In our study we found that the carrier dynamics in TaAs contains an extremely slow component, which could provide an explanation of the large time-integrated photocurrent reported in the literature [24].

V. CONCLUSION

In summary, we have performed TR spectroscopy on TaAs where the electrons are excited with an 800-nm pump pulse. In our experiment, we observed fast (~1 ps) and slow (~190 ps) relaxation in TaAs when probed at 560 nm. The time scale of the relaxation is consistent with the mechanism reported in the literature for TaAs [34]. The origin of this slow relaxation component is attributed to the low DOS near $E = 0$ and phonon reabsorption during carrier cooling. The fast and slow decay components correspond to e-h recombination and

e-ph coupling, respectively. Also, the relaxation times of both channels increase with increasing pump fluence due to the high carrier density. Furthermore, we found that upon changing the probing wavelength, from 560 to 525 nm, relaxation through e-ph coupling was not observable. This quenching of the e-ph relaxation channel is due to fewer electrons in the corresponding excited state immediately after thermalization, which allows all the carriers to relax through the more-efficient e-h recombination channel. An understanding of the carrier dynamics of TaAs might pave the way for its application in sensitive optoelectronics.

ACKNOWLEDGMENTS

We acknowledge funding from the Singapore Ministry of Education (MOE) AcRF Tier 1 [MOE2018-T1-1-097 and RG95/19 (S)] and Tier 3 (MOE2018-T3-1-002) and A*STAR PHAROS Programme on 2D Materials (SERC Grant No. 152 70 00016). Work at Los Alamos was carried out under the auspices of the US Department of Energy (DOE) National Nuclear Security Administration under Contract No. 89233218CNA000001 and was supported by the LANL LDRD Program. It was supported in part by the Center for Integrated Nanotechnologies, a DOE BES user facility.

[1] M. Z. Hasan and C. L. Kane, Rev. Mod. Phys. **82**, 3045 (2010).
[2] L. Fu, C. L. Kane, and E. J. Mele, Phys. Rev. Lett. **98**, 106803 (2007).
[3] S. Cai, J. Guo, V. A. Sidorov, Y. Zhou, H. Wang, G. Lin, X. Li, Y. Li, K. Yang, A. Li *et al.*, npj Quantum Mater. **3**, 62 (2018).
[4] X. Zhang, J. Wang, and S.-C. Zhang, Phys. Rev. B **82**, 245107 (2010).
[5] J. Yao, J. Shao, Y. Wang, Z. Zhao, and G. Yang, Nanoscale **7**, 12535 (2015).
[6] H. Zhang, X. Zhang, C. Liu, S.-T. Lee, and J. Jie, ACS Nano **10**, 5113 (2016).
[7] Y. Huang, Y. Song, S. Wang, I. Buyanova, and W. Chen, Nat. Commun. **8**, 15401 (2017).
[8] K. Vaklinova, A. Hoyer, M. Burghard, and K. Kern, Nano Lett. **16**, 2595 (2016).
[9] S. M. Hus, X.-G. Zhang, G. D. Nguyen, W. Ko, A. P. Baddorf, Y. P. Chen, and A.-P. Li, Phys. Rev. Lett. **119**, 137202 (2017).
[10] A. Dankert, J. Geurs, M. V. Kamalakar, S. Charpentier, and S. P. Dash, Nano Lett. **15**, 7976 (2015).
[11] Z. Wang, Y. Sun, X.-Q. Chen, C. Franchini, G. Xu, H. Weng, X. Dai, and Z. Fang, Phys. Rev. B **85**, 195320 (2012).
[12] Z. Liu, J. Jiang, B. Zhou, Z. Wang, Y. Zhang, H. Weng, D. Prabhakaran, S. Mo, H. Peng, P. Dudin *et al.*, Nat. Mater. **13**, 677 (2014).
[13] H. Yi, Z. Wang, C. Chen, Y. Shi, Y. Feng, A. Liang, Z. Xie, S. He, J. He, Y. Peng *et al.*, Sci. Rep. **4**, 6106 (2014).
[14] S. M. Young, S. Zaheer, J. C. Y. Teo, C. L. Kane, E. J. Mele, and A. M. Rappe, Phys. Rev. Lett. **108**, 140405 (2012).
[15] B.-J. Yang and N. Nagaosa, Nat. Commun. **5**, 4898 (2014).
[16] A. A. Zyuzin, S. Wu, and A. A. Burkov, Phys. Rev. B **85**, 165110 (2012).
[17] R. Wang, J. Z. Zhao, Y. J. Jin, W. P. Xu, L.-Y. Gan, X. Z. Wu, H. Xu, and S. Y. Tong, Phys. Rev. B **96**, 121104(R) (2017).
[18] S.-Y. Xu, I. Belopolski, N. Alidoust, M. Neupane, G. Bian, C. Zhang, R. Sankar, G. Chang, Z. Yuan, C.-C. Lee *et al.*, Science **349**, 613 (2015).
[19] G. Resta, S.-T. Pi, X. Wan, and S. Y. Savrasov, Phys. Rev. B **97**, 085142 (2018).
[20] X. Huang, L. Zhao, Y. Long, P. Wang, D. Chen, Z. Yang, H. Liang, M. Xue, H. Weng, Z. Fang *et al.*, Phys. Rev. X **5**, 031023 (2015).
[21] H. Weng, R. Yu, X. Hu, X. Dai, and Z. Fang, Adv. Phys. **64**, 227 (2015).
[22] Q. Ma, S.-Y. Xu, C.-K. Chan, C.-L. Zhang, G. Chang, Y. Lin, W. Xie, T. Palacios, H. Lin, S. Jia *et al.*, Nat. Phys. **13**, 842 (2017).
[23] S. I. Kimura, Y. Nakajima, Z. Mita, R. Jha, R. Higashinaka, T. D. Matsuda, and Y. Aoki, Phys. Rev. B **99**, 195203 (2019).
[24] S. Chi, Z. Li, Y. Xie, Y. Zhao, Z. Wang, L. Li, H. Yu, G. Wang, H. Weng, H. Zhang *et al.*, Adv. Mater. **30**, 1801372 (2018).
[25] S. Patankar, N. Nair, J. Analytis, J. Orenstein, and L. Wu, Proc. SPIE **10530**, 1053003 (2018).
[26] L. Wu, S. Patankar, T. Morimoto, N. L. Nair, E. Thewalt, A. Little, J. G. Analytis, J. E. Moore, and J. Orenstein, Nat. Phys. **13**, 350 (2017).
[27] K. Sun, S.-S. Sun, L.-L. Wei, C. Guo, H.-F. Tian, G.-F. Chen, H.-X. Yang, and J.-Q. Li, Chin. Phys. Lett. **34**, 117203 (2017).
[28] J. Buckeridge, D. Jevdokimovs, C. R. A. Catlow, and A. A. Sokol, Phys. Rev. B **93**, 125205 (2016).
[29] C. Zhang, C. Guo, H. Lu, X. Zhang, Z. Yuan, Z. Lin, J. Wang, and S. Jia, Phys. Rev. B **92**, 041203(R) (2015).
[30] I. Song, C. Park, and H. C. Choi, RSC Adv. **5**, 7495 (2015).
[31] K. Nagashino, T. Nishimura, K. Kita, and A. Toriumi, Appl. Phys. Express **2**, 025003 (2009).
[32] A. Rawat, N. Jena, Dimple, and A. De Sarkar, J. Mater. Chem. A **6**, 8693 (2018).
[33] N. Sirica, Y. M. Dai, L. X. Zhao, G. F. Chen, B. Xu, R. Yang, B. Shen, N. Ni, D. A. Yarotski, S. A. Trugman *et al.*, in *Conference on Lasers and Electro-Optics (CLEO)* (Optical Society of America, Washington, DC, 2018), paper FM1F.4.
[34] C. P. Weber, B. S. Berggren, M. G. Masten, T. C. Ogloza, S. Deckoff-Jones, J. Madéo, M. K. Man, K. M. Dani, L. Zhao, G. Chen *et al.*, J. Appl. Phys. **122**, 223102 (2017).
[35] Z. Li, H. Chen, S. Jin, D. Gan, W. Wang, L. Guo, and X. Chen, Cryst. Growth Des. **16**, 1172 (2016).
[36] Y. M. Sheu, Y. J. Chien, C. Uher, S. Fahy, and D. A. Reis, Phys. Rev. B **87**, 075429 (2013).
[37] I. Timrov, T. Kampfrath, J. Faure, N. Vast, C. R. Ast, C. Frischkorn, M. Wolf, P. Gava, and L. Perfetti, Phys. Rev. B **85**, 155139 (2012).
[38] J. M. Dawlaty, S. Shivaraman, M. Chandrashekhar, F. Rana, and M. G. Spencer, Appl. Phys. Lett. **92**, 042116 (2008).
[39] P. A. George, J. Strait, J. Dawlaty, S. Shivaraman, M. Chandrashekhar, F. Rana, and M. G. Spencer, Nano Lett. **8**, 4248 (2008).
[40] J. Fu, Q. Xu, G. Han, B. Wu, C. H. A. Huan, M. L. Leek, and T. C. Sum, Nat. Commun. **8**, 1300 (2017).

[41] J. Kim, J. Oh, C. In, Y.-S. Lee, T. B. Norris, S. C. Jun, and H. Choi, ACS Nano **8**, 2486 (2014).

[42] X.-C. Nie, H.-Y. Liu, X. Zhang, C.-Y. Jiang, S.-Z. Zhao, Q.-P. Zhao, F. Li, L. Yue, J.-Q. Meng, Y.-X. Duan *et al.*, Results Phys. **12**, 1089 (2019).

[43] A. Othonos, J. Appl. Phys. **83**, 1789 (1998).

[44] B. M. Fregoso, Phys. Rev. B **100**, 064301 (2019).

[45] E. Vella, H. Li, P. Grégoire, S. M. Tuladhar, M. S. Vezie, S. Few, C. M. Bazán, J. Nelson, C. Silva-Acuña, and E. R. Bittner, Sci. Rep. **6**, 29437 (2016).

Correction: The order of the sixth and eighth authors has been interchanged. An email address was added for the eighth author.